

STRUCTURE AND POPULATION OF THE NGC55 STELLAR HALO FROM A SUBARU/SUPRIME-CAM SURVEY¹

MIKITO TANAKA², MASASHI CHIBA², YUTAKA KOMIYAMA³, PURAGRA GUHATHAKURTA⁴, AND JASON S. KALIRAI⁵

Draft version October 26, 2018

ABSTRACT

As part of our survey of galactic stellar halos, we investigate the structure and stellar populations of the northern outer part of the stellar halo in NGC 55, a member galaxy of the Sculptor Group, using deep and wide-field V - and I -band images taken with Subaru/Suprime-Cam. Based on the analysis of the color-magnitude diagrams (CMDs) for red-giant-branch (RGB) stars, we derive a tip of RGB (TRGB)-based distance modulus to the galaxy of $(m-M)_0 = 26.58 \pm 0.11$ ($d = 2.1 \pm 0.1$ Mpc). From the stellar density maps, we detect the asymmetrically disturbed, thick disk structure and two metal-poor overdense substructures in the north region of NGC 55, which may correspond to merger remnants associated with hierarchical formation of NGC 55's halo. In addition, we identify a diffuse metal-poor halo extended out to at least $z \sim 16$ kpc from the galactic plane. The surface-brightness profiles toward the z -direction perpendicular to the galactic plane suggest that the stellar density distribution in the northern outer part of NGC 55 is described by a locally isothermal disk at $z \lesssim 6$ kpc and a likely diffuse metal-poor halo with V -band surface brightness of $\mu_V \gtrsim 32$ mag arcsec⁻², where old RGB stars dominate. We derive the metallicity distributions (MDs) of these structures on the basis of the photometric comparison of RGB stars with the theoretical stellar evolutionary models. The MDs of the thick disk structures show the peak and mean metallicity of $[\text{Fe}/\text{H}]_{\text{peak}} \sim -1.4$ and $[\text{Fe}/\text{H}]_{\text{mean}} \sim -1.7$, respectively, while the outer substructures show more metal-poor features than the thick disk structure. Combined with the current results with our previous study for M31's halo, we discuss the possible difference in the formation process of stellar halos among different Hubble types.

Subject headings: galaxies: individual (NGC 55) — galaxies: halos — galaxies: structure

1. INTRODUCTION

Our understanding of how a stellar halo surrounding a disk galaxy like the Milky Way has formed is still enigmatic, because the observational information of this faint galactic component is yet limited, except for Local Group galaxies. Halo stars in the Milky Way are characterized by low metal abundance and high velocity dispersion and this extreme nature reflects the early chemo-dynamical evolution of the Milky Way. Extensive analyses of these stars have revealed, e.g., the dual nature of the halo structure (inner flattened halo in prograde rotation and outer spherical halo in retrograde rotation) (e.g., Carollo et al. 2007). Also, recent growing observational evidence suggests that the Milky Way halo has formed from an assembly process of many subsystems, as deduced from stream-like halo substructures (e.g., Yanny et al. 2000). Similar substructures have also been identified in M31's halo, including the Giant Stellar Stream (Ibata et al. 2007). Indeed, M31's halo provides a clear external view of ancient stellar populations: the halo is found to be extended more than 150 kpc (Guhathakurta et al. 2005) and has character-

istic spatial structure and metallicity distributions (e.g., Kalirai et al. 2006; Ibata et al. 2007; Tanaka et al. 2010). Another Local Group galaxy, M33, seems to have a rather smooth halo, although its disk orientation prevents the more refined picture of the halo. Thus, detailed studies of old stellar halos in various-type galaxies provide us with important clues to the understanding of galaxy formation.

Exploring stellar halos even beyond the Local Group is of great importance to accomplish our understanding of their generic nature and past formation history in different disk galaxies at different environments. Model investigations (e.g., Kauffmann 1996) predict that each disk galaxy has been developed through a different formation and evolutionary path: the collapse epoch, star formation history, and assembly rate of subsystems are not common and each stellar halo is expected to hold a different morphology, as other components (bulge and disk) differ along the Hubble sequence.

In this regard, an edge-on spiral SB(s)m galaxy, NGC 55, which is a member of the nearby Sculptor group that consists of approximately 30 galaxies (Côté et al. 1997; Jerjen et al. 2000), is an excellent test-bed for this study: it provides an external perspective of a nearby late-type disk galaxy and yet is close enough to resolve individual stars. For example, NGC 55 shows asymmetric extra-planar morphology as derived from emission-line images (Ferguson et al. 1996) and its nuclear source shows, based on far-infrared measurements, energetic star formation rate, which is of comparable luminosity to the bright star formation regions at the center of M33 and the Milky Way (Engelbracht et al. 2004). Based on the

¹ Based on data collected at the Subaru Telescope, which is operated by the National Astronomical Observatory of Japan.

² Astronomical Institute, Tohoku University, Aoba-ku, Sendai 980-8578, Japan (current address); mikito@astr.tohoku.ac.jp

³ National Astronomical Observatory of Japan, 2-21-1 Osawa, Mitaka, Tokyo 181-8588, Japan

⁴ University of California Observatories/Lick Observatory, University of California Santa Cruz, 1156 High Street, Santa Cruz, California 95064, USA

⁵ Space Telescope Science Institute, Baltimore, MD 21218

observational study of asymptotic giant branch (AGB) stars, Davidge (2005) found that there are no evidence for a young or intermediate-age component in the extra-planar region such as 2 kpc off of the disk plane, suggesting that the population has ages of about 10 Gyr. On the other hand, Tikhonov et al. (2005) found an exponential spatial distribution of RGB stars between 2 and 7 kpc from the center along the minor axis, using HST/WFPC2. Seth et al. (2005a,b), as part of a snapshot survey of 16 nearby edge-on late-type galaxies, observed the thin disk of NGC 55 using HST/ACS. They determined the fundamental properties of the resolved stellar population such as the distance, MD and spatial distributions of main-sequence, AGB and RGB stars in the inner part at $z \lesssim 1.5$ kpc. However, since all the previous studies using HST are restricted to a small field-of-view, the global structure of an outer part of NGC 55 is yet unknown. Therefore, we conduct a high-resolution, deep wide-field survey of the halo of NGC 55 using Subaru/Suprime-Cam, to elucidate its fundamental properties for the first time.

The layout of this paper is as follows. In Section 2, we present observations and summarize procedures for performing photometry for our Suprime-Cam data. Sections 3, 4 and 5 are devoted to our results for quantitative analysis of the CMDs of NGC 55's stellar populations, including the distance estimate using the TRGB stars, the detection of substructures in NGC 55's halo from the stellar population maps, the radial profiles of the resolved stars, and their MDs using the theoretical isochrones. In Section 6, comparing with previous studies on stellar halos, we discuss the implications of our results and conclusions are drawn.

2. DATA

In this study, we use the Suprime-Cam imager (Miyazaki et al. 2002) on the 8.2-m Subaru Telescope on Mauna Kea in Hawaii. Suprime-Cam consists of ten 2048×4096 CCDs with a scale of $0''.202$ per pixel and covers a total field-of-view of $34' \times 27'$. We have observed the north part of a stellar halo in NGC 55 in 2009 December. Figure 1 shows the location of our Suprime-Cam pointing containing the edge of NGC 55's thick disk suggested by Tikhonov et al. (2005) and the outer halo out to around 17 kpc perpendicular to the galactic plane. In this study, we define that x -axis corresponds to the galactic major axis, and z -axis which is converted based on the inclination (80°) in a direction perpendicular to the galactic mid-plane. The observations were made with Johnson V -band and Cousins I -band filters. Exposure times of our targeted fields are 960 sec and 1800 sec in V and I -band, respectively. The weather condition was photometric but slightly poor, with seeing of around $1''.0$. To estimate the number of foreground stars of the Milky Way and unresolved background galaxies in each NGC 55's field, we also obtained the imaging data for the control field, which is located at the same galactic latitude ($b \sim -76^\circ$) as the object field, but is about 3° away from it.

We have performed reduction, photometry and artificial star experiments following the same manner as given in Tanaka et al. (2010). The raw data were reduced in the standard procedures, with the software package SDFRED, a useful pipeline developed to optimally deal with Suprime-Cam images (Yagi et al. 2002; Ouchi et al.

2004). We then conducted PSF-fitting photometry using the IRAF version of the DAOPHOT-II software (Stetson 1987). Comparing input artificial stars with output ones, we evaluated incompleteness due to low S/N ratio and selection criteria based on DAOPHOT parameters. Then, the 50% (80%) completeness of the object field for each filter is reached at $V_{\text{NGC55}}^{50} = 25.61$ ($V_{\text{NGC55}}^{80} = 25.03$) and $I_{\text{NGC55}}^{50} = 25.07$ ($I_{\text{NGC55}}^{80} = 24.40$) in the nearest field to the NGC 55 center, while the completeness of the control field reached at $V_{\text{Control}}^{50} = 25.80$ ($V_{\text{Control}}^{80} = 25.23$) and $I_{\text{Control}}^{50} = 25.27$ ($I_{\text{Control}}^{80} = 24.61$). The typical mean magnitude errors at the 50% (80%) completeness limits, based on the simulated numerous stars, are of the order of $\sigma_V \sim 0.3$ (0.2) and $\sigma_I \sim 0.3$ (0.2).

Brief information about NGC 55 and the references are given in Table 1. Reddening correction is applied to this Suprime-Cam field based on the extinction maps of Schlegel et al. (1998), and the Dean et al. (1978) reddening law $E(V-I) = 1.34E(B-V)$ and $A_I = 1.31E(V-I)$. The central coordinate of NGC 55 is derived from 2MASS observations, in agreement with the peak position of the blue light and also the location of maximum symmetry of H_I velocity field as described in Hummel et al. (1986). In addition, the galaxy's circular velocity, inclination and position angle are derived from their neutral hydrogen and radio continuum observations.

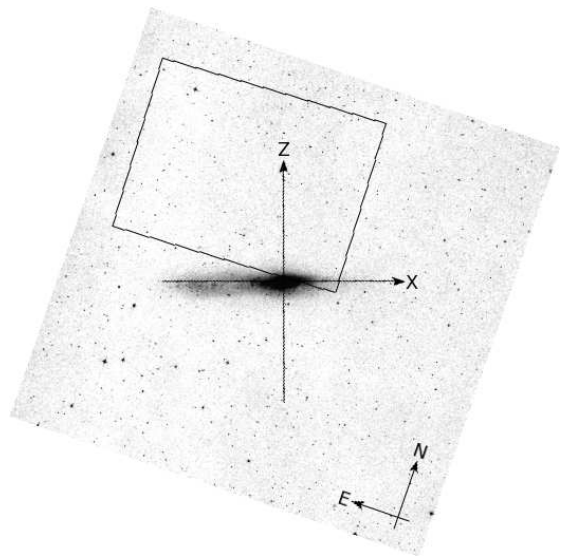


FIG. 1.— The locations and field of view of our Subaru/Suprime-Cam field, overlaid on a red Digitized Sky Survey image of NGC 55 covering about $60' \times 60'$. A rectangle shows an area in which we analyzed our Suprime-Cam data, corresponding to 0.22 square degrees.

3. DISTANCE TO NGC 55

Figure 2 shows the typical CMDs for stellar-like sources in the inner and outer region of NGC 55's halo (left and middle) and for the control field (right), after removing extended sources such as background galaxies and cosmic rays based on DAOPHOT parameters. The three CMDs have the same sky coverage of 0.022 square degrees. The solid lines in the CMDs show theoretical RGB tracks from VandenBerg et al. (2006) for an age of 12 Gyr, $[\alpha/\text{Fe}] = +0.3$, and metallicities (left to right) of $[\text{Fe}/\text{H}] = -2.31, -1.71, -1.31, -1.14, -0.71$ and -0.30 .

TABLE 1
PROPERTIES OF NGC 55

Property	Value	Reference
RA (J2000)	00 ^h 14 ^m 53 ^s .6	NED
Dec (J2000)	−39°11′48″.0	NED
Morphological type	SB(s)m:sp	NED
A_I	0.024	Schlegel et al. (1998)
V_{circ} (km s ^{−1})	110	Hummel et al. (1986)
Inclination	80°	Hummel et al. (1986)
Position Angle	109°	Hummel et al. (1986)
$(m - M)_0$	26.58 (2.1 Mpc)	this work

The dashed lines denote about 50% and 80% completeness limits as determined by artificial star experiments.

The clearest feature in the inner region of NGC 55’s halo is a metal-poor RGB with $-2.3 < [\text{Fe}/\text{H}] < -1.1$. Furthermore, at $I \sim 22.5$, we also recognize a tip of RGB (TRGB). The stars distributed in the brighter part than the TRGB magnitude are probably metal-rich and/or young stellar population in the thermally pulsating AGB phase (TPAGB). In contrast, it seems that the CMD of the outer region is rather similar to that of the control field, suggesting that there might be only a little intrinsic halo population in this outer field beyond $z \sim 12$ kpc from the NGC 55 center.

The TRGB is a useful indicator to estimate the distance to resolved galaxies (Salaris & Cassisi 2005). If there are a sufficient number of old and metal-poor RGB stars in a targeted field, the TRGB is easily detected as a sharp cutoff of the luminosity function (LF) with the application of an edge-detection algorithm, the Sobel filter (e.g., Salaris & Cassisi 2005; Tanaka et al. 2010).

Detection of the TRGB is shown in Figure 3. The LF around the TRGB magnitude is derived from the selected RGB stars in a lower metallicity range than $[\text{Fe}/\text{H}] = -0.7$ to minimize the effect of empirical calibration of the TRGB magnitude. The LF is gradually standing up at $I_0 \sim 21.7$ because of the increase of TPAGB stars and steeply rising up at $I_0 = 22.48 \pm 0.05$. The TRGB magnitude suffers from statistical uncertainty of the order of about 0.05 mag. In estimating the extinction-corrected apparent magnitude of TRGB, systematic errors also arise in association with zero point uncertainties, aperture corrections, photometric errors, smoothing of the LFs and extinction law; the resultant total error is evaluated by an rms of these errors. We further conduct 1,000 Monte Carlo realizations of the data, such that the brightness of each object is re-distributed in the form of a Gaussian distribution with standard deviation equal to the photometric error. It is found that the resultant deviation of the TRGB magnitude is only as small as 0.03 mag and thus reasonably small.

On the assumption that the absolute I_0 -band magnitude of the TRGB is $M_I^{\text{TRGB}} = -4.1 \pm 0.1$ for metal-poor TRGB stars, the distance modulus (e.g., Salaris & Cassisi 2005) is 26.58 ± 0.11 corresponding to 2.1 ± 0.1 Mpc. This value is consistent with previous studies based on the same TRGB method as this study (Seth et al. 2005a; Tikhonov et al. 2005).

4. STELLAR POPULATION MAPS

In this section, we investigate how the stellar populations of NGC 55’s halo are distributed spatially out to about 17 kpc from NGC 55’s center. To do so, we draw stellar density maps corresponding to each stellar population, based on the matched filter method explained in our previous study (Tanaka et al. 2010). First, we visually separate the two major structures (thick disk and diffuse halo) and some substructures from the following spatial distributions of stellar population of NGC 55. Then, we quantitatively discriminate the difference of their populations based on their CMDs and MDs.

Figure 4 shows density maps of RGB stars in the north halo region of NGC 55, divided $[\text{Fe}/\text{H}]$ into two non-overlapping ranges (left panel: $[\text{Fe}/\text{H}] < -2.01$, right panel: $-2.01 < [\text{Fe}/\text{H}]$, see also Figure 2). Then, we impose several criteria to get rid of unpleasant contaminations unrelated to the RGB stars from our photometric catalog: for example, appropriate color, magnitudes between the TRGB and 80% completeness. In addition, to remove the remaining background and foreground contaminations, we subtract the constant value estimated based on the data of the control field from each bin of the stellar maps. The background levels for RGB and AGB stars are $\mu_{V,\text{back}}^{\text{RGB}} \sim 30.8 \pm 0.1$ mag arcsec^{−2} and $\mu_{V,\text{back}}^{\text{AGB}} \sim 33.6 \pm 0.1$ mag arcsec^{−2}, respectively.

4.1. Inner Structures

Both panels of Figure 4 show that NGC 55 has an asymmetric stellar structure in eastern and western regions, regardless of metal abundances. There is a somewhat extended structure towards the z -direction in the eastern part. We nominally refer the eastern and western structures to as “Thick Disk East (TDE)” and “Thick Disk West (TDW)”, respectively hereafter. TDE seems to be related to the disturbed eastern disk which is in the shape of a tadpole tail, as seen in Figure 1. This might suggest that an accreted satellite galaxy gave a structural influence on the eastern part of the disk structure (e.g., Abadi et al. 2003; Yoachim & Dalcanton 2006).

In contrast, assuming that TDW, which is a high density region in the north-western part of NGC 55, is undisturbed, we regard this region as the normal thick disk. The scale height of the plausible thick disk of NGC 55 is estimated as $z_{0,\text{thick}} \sim 1.6$ kpc (see also Figure 9), which is consistent with that estimated by the previous HST study (Tikhonov et al. 2005). In fact, considering $V_{\text{circ}} = 110$ km s^{−1}, the estimated scale height is in good agreement with the relation between galactic rotational velocity and scale-height of thin/thick disk constructed by Yoachim & Dalcanton (2006) (see their Fig. 9).

Next, we compare stellar populations between TDE and TDW, based on their CMDs shown in Figure 5. There are well-populated RGB stars in both CMDs, suggesting that a dominant population in both structures is old and metal-poor with $[\text{Fe}/\text{H}] < -1$. Furthermore, it is remarkable that AGB stars exist above the TRGB magnitude of $I_0 = 22.48$ as also shown in the previous section. The AGB population of TDE seems to be more sharply rising at $(V - I) \sim 1.6$ compared to that of TDW. If this feature is real, it indicates that the stellar population of TDE is different from that of TDW: the former is possibly several Gyr younger than the latter. However, color distributions of both TDE and TDW

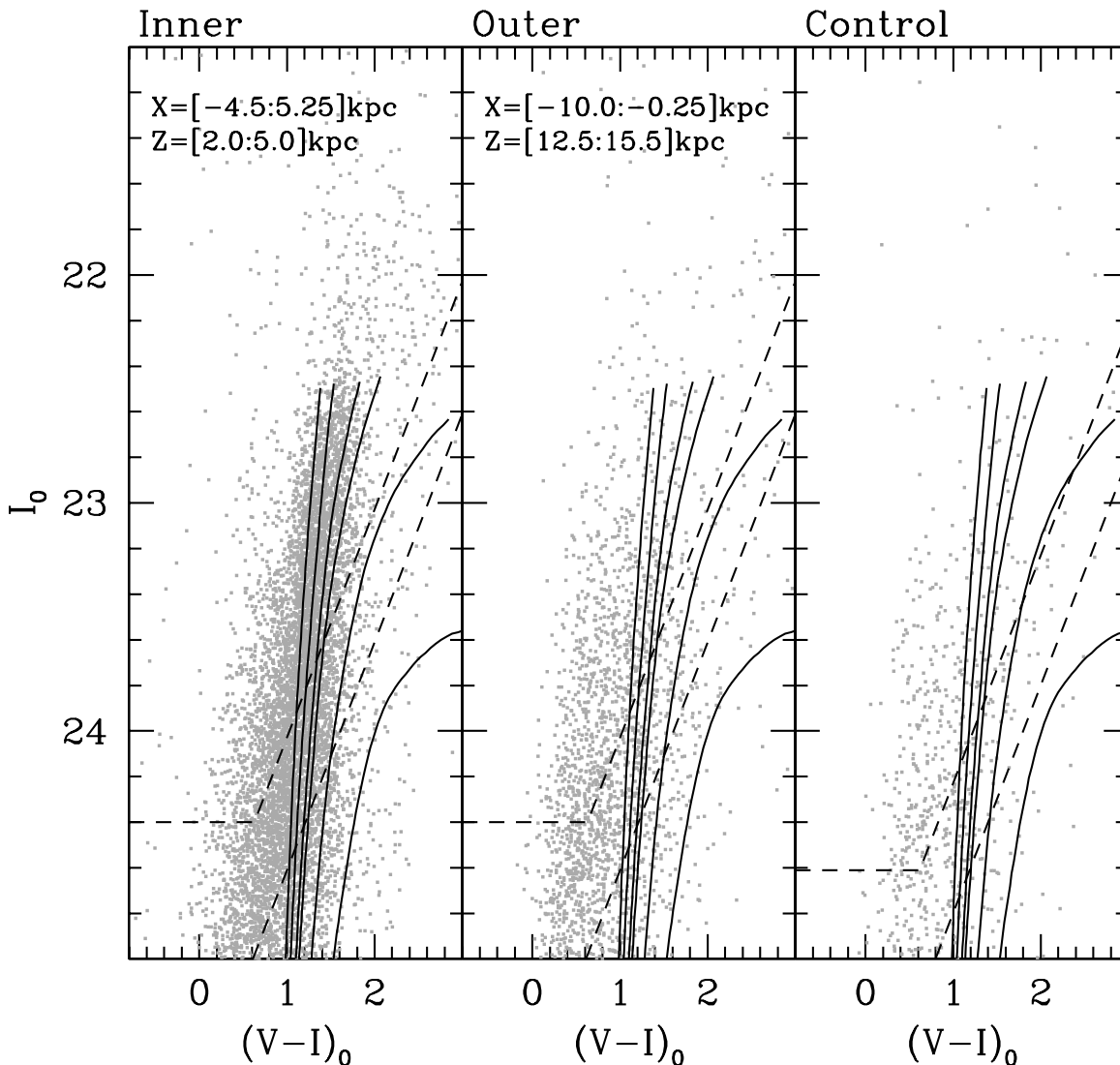


FIG. 2.— $[(V-I)_0, I_0]$ color-magnitude diagrams for stellar-like sources in the inner and outer regions of NGC 55’s halo (left and middle) and the control field (right). The solid lines are theoretical isochrones (VandenBerg et al. 2006) of age 12 Gyr and $[\alpha/\text{Fe}] = +0.3$ spanning the metallicity range $[\text{Fe}/\text{H}] = -2.31, -1.71, -1.31, -1.14, -0.71$ and -0.20 . The dashed lines denote the full ranges of the 50% and 80% completeness levels.

at $21.00 < I_0 < 22.48$ have a similar shape and peak at $(V-I)_0 \sim 1.7$. Also, the ratio of the number of AGB stars at $21.0 < I_0 < 22.48$ and $0.6 < (V-I)_0 < 2.5$ to that of bright RGB stars at $22.48 < I_0 < 23.0$ and $0.6 < (V-I)_0 < 2.0$ is evaluated as about 30% for both TDE and TDW, where the effect of contaminations is limited within their Poisson noise. Thus, population difference between TDE and TDW would not be significant from the current CMD analysis, so that that bulk populations in TDE and TDW may originate from the same, pre-existing disk component.

4.2. Outer Structure

Despite metallicity cuts, the stellar density rapidly declines to a background level beyond $z \sim 5$ kpc, according to the stellar density maps of Figure 4. However, metal-poor stars are diffusely distributed in the outer part of the halo. The left panel of Figure 6 shows a CMD in the outer part of NGC 55 which is enclosed by the largest rectangle in the metal-poor stellar density map of Fig-

ure 4, whereas the right panel presents a CMD in the control field with the same area of a field-of-view as the left panel. Although both of the CMDs contain numerous background contaminations below $I_0 \sim 23$, the CMD of NGC 55’s outer part seems to have a metal-poor population with $[\text{Fe}/\text{H}] \lesssim -2$ like the diffuse outer halo of M31 and the Milky Way. The existence of this metal-poor population in the outer halo can be verified by comparing both CMDs at bright and metal-poor RGB part of $(V-I)_0 \sim 1.2$ and $I_0 \sim 22.8$ (corresponding to dashed boxes in the CMDs). In fact, the number of the stellar objects inside this box in the outer halo field of NGC 55 ($n_{\text{halo}} = 69$) is more than those in the control field ($n_{\text{control}} = 43$), i.e., well beyond the Poisson noise. This fact that the diffuse halo extends to the outer part of NGC 55 is consistent with the suggestion of the previous HST study (Tikhonov et al. 2005). However, since its signal-to-noise ratio is not high (of ~ 3), further observations at other wavelengths are needed to reduce the

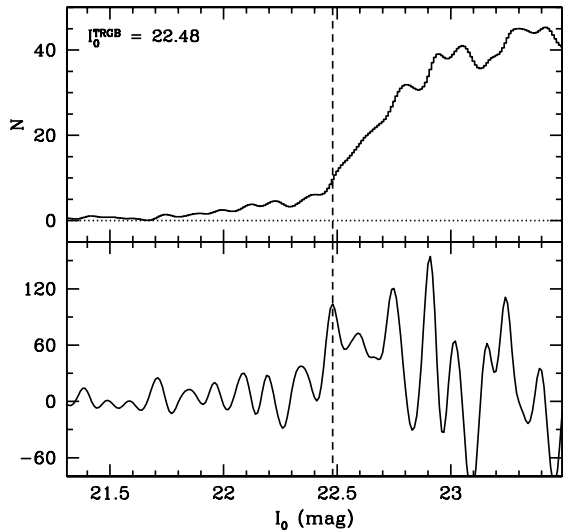


FIG. 3.— TRGB detection in NGC 55. The upper panel presents the smoothed LFs as a function of the incompleteness-corrected and background-subtracted I_0 -band magnitude zoomed in around the TRGB magnitude. The lower panel indicates the Sobel filter response to the LF. The vertical dashed line shows the derived TRGB magnitude.

contamination of unresolved background galaxies and to confirm the presence of this halo component.

In addition, two regions showing significant excess of stellar density beyond the level of the diffuse halo can be identified in the north-east field of NGC 55 (right panel of Figure 4), which we refer to as Substructure 1 and 2 hereafter. These halo substructures are more clearly presented in Figure 7, which shows a background-subtracted surface brightness profile in the same direction as the major axis at $5.25 < z < 7.25$ kpc: the surface brightness is estimated using the resolved RGB stars selected as $(V_0, I_0) < (25.03, 24.40)$, i.e., brighter magnitude than 80% completeness limit (see also Section 6). The error bars are estimated from the square root of the number counts including both stellar and background flux. The profile shows the presence of two overdense regions beyond the Poisson noise at $x \sim 2.5$ kpc and $x \sim 8$ kpc bounded by vertical gray dotted lines. The CMDs of both substructures (Figure 8) show a similar distribution of RGB stars including the presence of metal-poor stars with $-2.3 \lesssim [\text{Fe}/\text{H}] \lesssim -1.7$, although these substructures are spatially separated as shown in Figure 7. The difference of stellar population between these substructures will be more quantitatively examined based on the analysis of their MDs in Section 5.

4.3. Surface Brightness Profile

To further investigate NGC 55's global structure, we investigate the distribution of surface brightness for the resolved RGB stars using those brighter than 80% completeness limit. Figure 9 shows surface brightness profiles converting the summed-up flux counts of selected stars to the surface brightness in mag arcsec^{-2} , and subtracting the surface brightness of the control field, for which remaining foreground and background contaminations are removed based on the statistical method (Tanaka et al. 2010). The error bars are estimated from the square

root of the number counts including both stellar and background flux. Black and gray circles show the surface brightness profiles at $0 < x < 4$ kpc (where stars in TDW dominate) and $-5 < x < -1$ kpc (where those in TDE dominate), respectively. It is noted that in the latter profile, there is a prominent overdense structure (corresponding to Sub 1) at $z \sim 6$ kpc, as also mentioned in the previous subsection.

It also follows from the figure that the thick disk component is extended at least up to about 5 kpc, as represented by isothermal disk models (dashed lines): the vertical profile of a disk structure is defined as (van der Kruit & Searle 1981):

$$\Sigma(z) \propto \text{sech}^2\left(\frac{z}{z_0}\right) \quad (1)$$

where $\Sigma(z)$ is the surface brightness or density at a position z above the midplane and z_0 is the scale height. As discussed in Section 4.1, the scale height of TDW is $z_{0,\text{RGB}}^{\text{W}} = 1635 \pm 30$ pc which is a typical value for a late-type galaxy with $V_{\text{circ}} = 110$ km s^{-1} (Yoachim & Dalcanton 2006). However, on the assumption that NGC 55 has slower rotational velocity like $60 \lesssim V_{\text{circ}} \lesssim 90$ km s^{-1} (e.g., Puche et al. 1991), it has a somewhat thicker disk. Nonetheless, it is notable that the thick disk profile in the eastern part (TDE) has a significantly larger scale height, $z_{0,\text{RGB}}^{\text{E}} = 2203 \pm 25$ pc, than in the western part (TDW), implying that the eastern thick disk has been heated up by the interaction with an accreted dwarf galaxy in the Sculptor group.

Regarding the surface brightness profile of the bright AGB stars (fitted with dotted lines in the figure), we obtain the scale heights of $z_{0,\text{AGB}}^{\text{W}} = 969 \pm 62$ pc and $z_{0,\text{AGB}}^{\text{E}} = 1341 \pm 60$ pc, respectively, for the north-western and north-eastern regions of NGC 55. As reported by previous studies of NGC 55 and other galaxies (Seth et al. 2005b; Tikhonov et al. 2005), the intermediate-age AGB stars in spiral galaxies show steeper spatial gradients in their number density than the old RGB stars and thus are almost absent in the outskirts of galaxies. This result strongly suggests the presence of an older component with a larger scale height in the outer part of the disk as investigated in Seth et al. (2005b). Furthermore, the old RGB populations have a scale height similar to typical thick disk components, whereas the intermediate-age stellar population has a scale height very similar to typical thin disk components; this is consistent with the more systematic consideration of Yoachim & Dalcanton (2006). Therefore, assuming our AGB population more clearly traces the thin disk of NGC 55, the eastern part of the thin disk in NGC 55 may have been dynamically heated by merging satellites, forming a thicker disk as seen in the eastern part. In addition, the fact that the scale height we calculated based on AGB is somewhat larger than that of the more inner eastern disk estimated by Seth et al. (2005b) supports that the outer intermediate-age disk is more significantly expanded. Therefore, NGC 55's disk may be extended toward a large height at around 4 kpc from the galactic plane.

Finally, we investigate the remote outer region of the diffuse halo of NGC 55 at $z \gtrsim 8$ kpc. Tikhonov et al. (2005) reported that there is a transitional point from

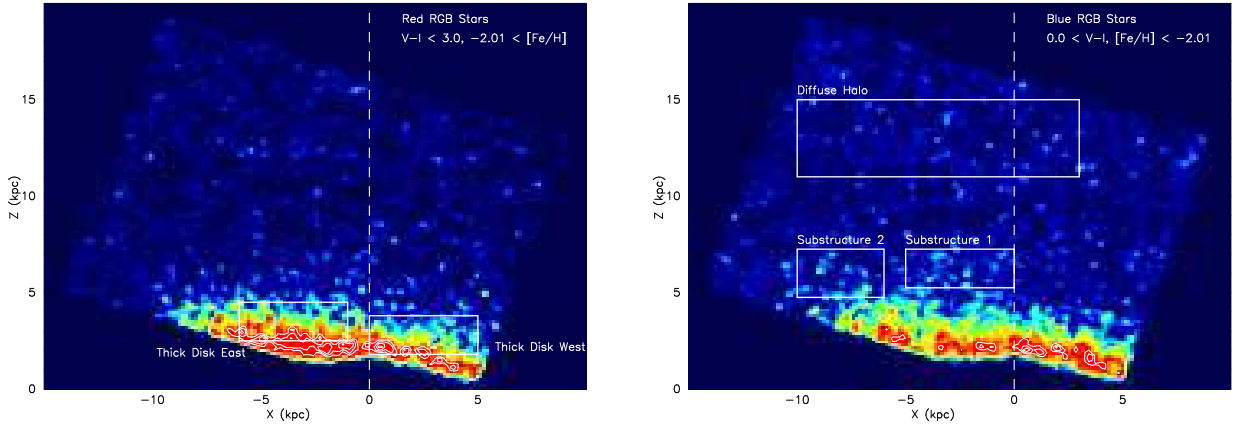


FIG. 4.— Log-scaled matched filter maps to a limiting magnitude of $I_0 = 24.4$ and $V_0 = 25.0$. The left panel shows the distribution of red RGB stars chosen with $(V - I) < 3.0$ and $-2.01 < [\text{Fe}/\text{H}]$, while the right panel is for blue RGB stars with $0.0 < (V - I)$ and $[\text{Fe}/\text{H}] < -2.01$. The resolution of this map is $0.15^\circ \times 0.15^\circ$ pixels, smoothed with a Gaussian kernel over 3 pixels.

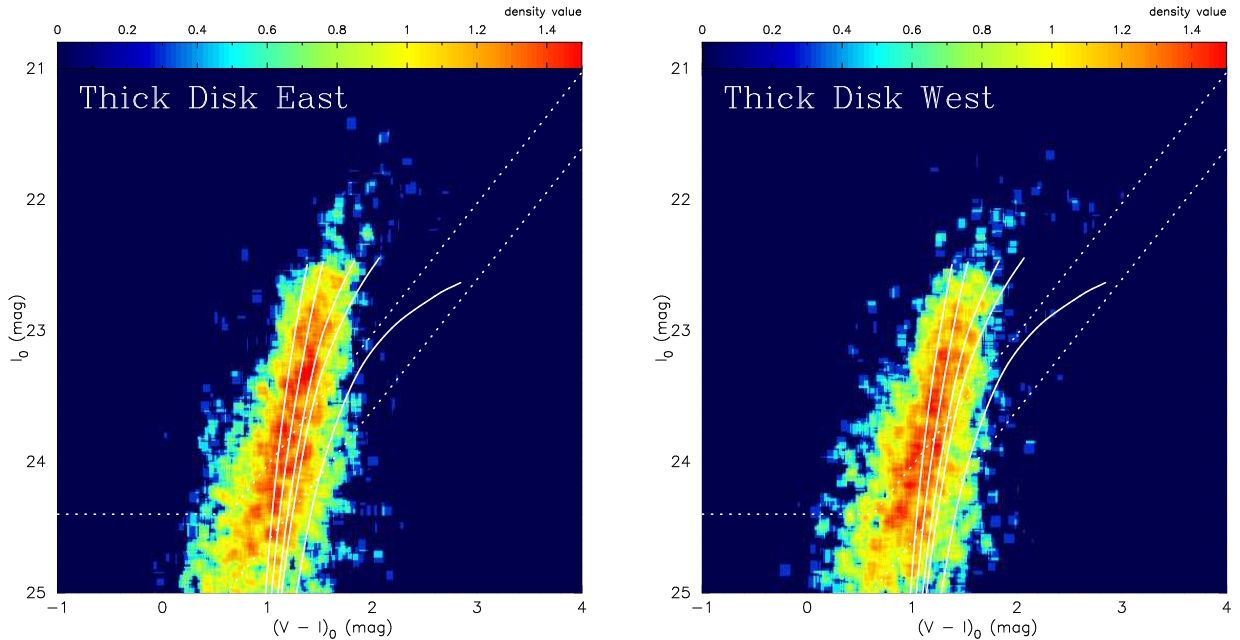


FIG. 5.— $[(V - I)_0, I_0]$ color-magnitude diagrams for stellar-like sources in TDE (left) and TDW (right) regions of NGC 55. The solid lines are theoretical isochrones (VandenBerg et al. 2006) of age 12 Gyr and $[\alpha/\text{Fe}] = +0.3$ spanning the metallicity range $[\text{Fe}/\text{H}] = -2.31, -1.71, -1.31, -1.14$ and -0.71 . The dotted lines denote the full ranges of the 50% and 80% completeness levels.

the disk to the halo at 6.5 kpc based on the deviation of their estimated density distribution from the starlight (see their Figure 12). However, considering our surface brightness profile shown in Figure 7 and 9, it is likely that the deviation is attributable to the overdense substructure of Sub 2, taking into account their HST/WFPC2 pointings on the minor axis of NGC 55. In fact, as discussed in Section 4.2, the outer halo of NGC 55 is substantially diffuse, and seems to have a nearly flat profile below the background level, $\mu_{V,\text{back}}^{\text{RGB}} \sim 30.8 \pm 0.1$ mag arcsec $^{-2}$. Taking into account this faintness and spatial profile of the NGC 55's halo, its total mass may be smaller than that of M31, like halos in other late-type galaxies such as M33 and LMC. It is noted that the presence of more substructures at a more remote field from the galaxy center ($z \sim 12$ kpc) may be likely if the halo

of NGC 55 also originates from accretion of many dwarf galaxies, as suggested for bright spirals like M31 and the Milky Way (Bullock & Johnston 2005). However, to assess this picture, further observations of the outer halo of NGC 55 are necessary.

5. METALLICITY DISTRIBUTIONS

In this section, we discuss the difference of stellar populations between the above-mentioned substructures, based on the comparison for the MDs of the RGB stars. To construct MDs, we adopt the Victoria-Regina theoretical isochrones from VandenBerg et al. (2006) (see also Tanaka et al. 2010). In accordance with the interpolation and extrapolation scheme of Kalirai et al. (2006), we calculate the metallicity for each star in the same segment of the CMD, assuming stellar population with

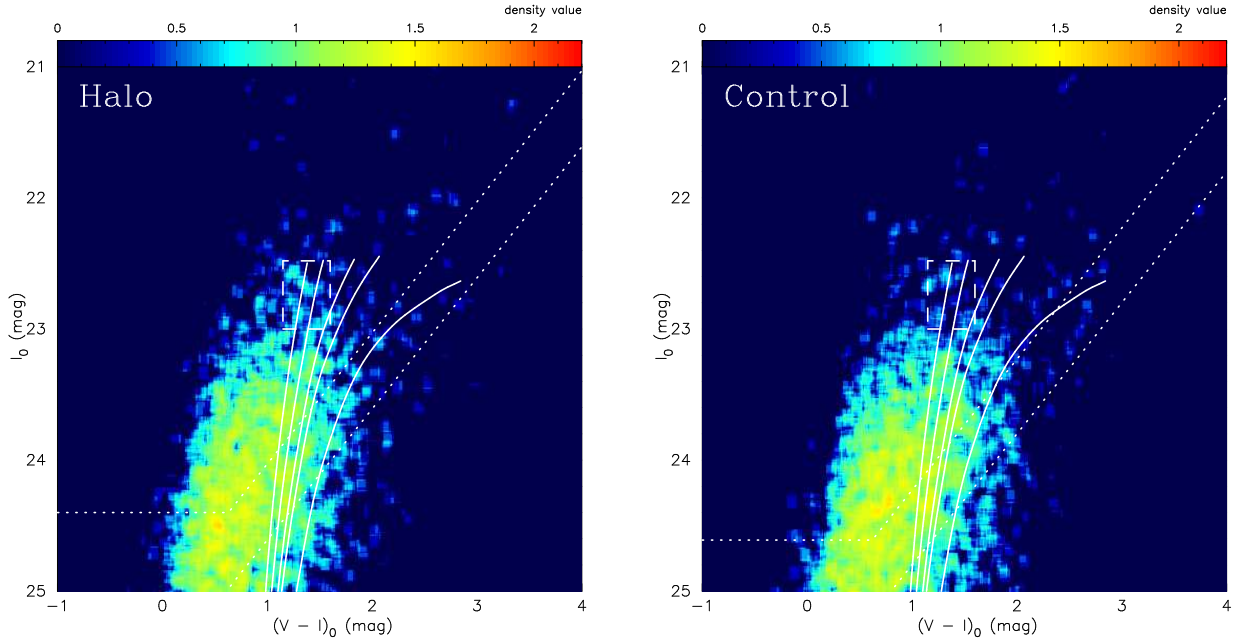


FIG. 6.— $[(V - I)_0, I_0]$ CMDs for stellar-like sources in the NGC 55's halo (left) and the control field (right). The solid lines are theoretical isochrones (VandenBerg et al. 2006) of age 12 Gyr and $[\alpha/\text{Fe}] = +0.3$ spanning the metallicity range $[\text{Fe}/\text{H}] = -2.31, -1.71, -1.31, -1.14$ and -0.71 . The dotted lines denote the full ranges of the 50% and 80% completeness levels. The existence of metal-poor population in the halo field can be identified by comparing the number of RGB stars within the dashed boxes between these panels (see text for more details).

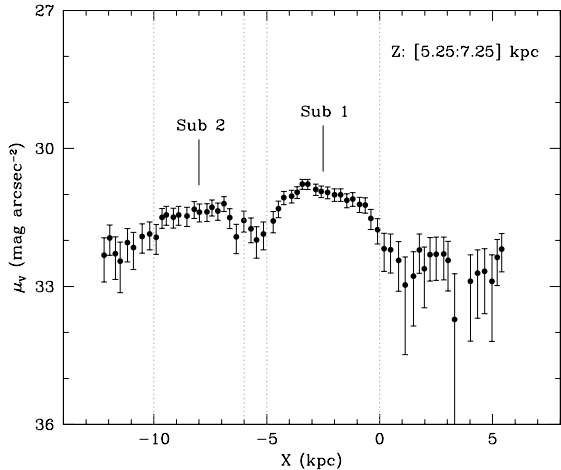


FIG. 7.— The surface brightness profile in the same direction as the major axis at $5.25 < z < 7.25$ kpc. Two overdense regions bounded by vertical gray dotted lines are regarded as substructures, Sub 1 and Sub 2, which are also denoted in the stellar density map (right panel in Figure 4).

$[\alpha/\text{Fe}] = +0.3$, age of 12 Gyr and the same distance modulus of 26.58 estimated in § 3. Furthermore, for secure determinations of MDs, we select the targeted RGB stars having $22.48 < I_0 < 23.48$ and $1.05 < (V - I)_0 < 2.2$. These selection criteria allow us to remove a number of contaminations, such as AGB stars, young stars and background galaxies. After performing the interpolation procedure for our photometric data, we subtract the MD of the control field from that of each object field in order to remove the effects of the remaining contaminations.

Since the MD of the control field shows a nearly flat distribution within the Poisson errors in the effective metallicity range of $-2.8 \lesssim [\text{Fe}/\text{H}] \lesssim -0.7$ (gray histograms in Figure 10), this subtraction procedure does not affect the determination for the intrinsic shape of NGC 55's MDs. In addition, the fraction of the contaminations is estimated as roughly 30% in Sub 2 field with the smallest statistic, whereas it is no more than 6% in TDE with the highest statistic.

Figure 10 shows the resultant contaminations-subtracted MDs for the four substructures we have newly identified in this study. The vertical error bars denote a nominal uncertainty in each metallicity bin as derived from the Poisson errors. For reference, we also plot the MD of the control field (consisting of 69 objects) by a gray histogram, which clearly shows a nearly flat distribution within the Poisson errors. The vertical dotted lines correspond to the values of mean (black) and median (gray) metallicity in each substructure, which are also summarized in Table 2. It follows that the MDs of TDE and TDW with high stellar density have a more metal-rich peak ($[\text{Fe}/\text{H}]_{\text{peak}} \sim -1.4$) than those of Sub 1 and 2 with low stellar density. All the MDs show a somewhat broad distribution ranging from $[\text{Fe}/\text{H}] \sim -3$ to ~ -1 . For comparison, we also plot the MD for the Giant Southern Stream observed in M31's halo (Tanaka et al. 2010) (gray dashed histogram), which is clearly different from the MDs in NGC 55. It is also worth comparing with the MDs of NGC 55's thin disk ($[\text{Fe}/\text{H}]_{\text{mean}}^{\text{thin}} \sim -1.0$) as obtained by Seth et al. (2005b) (see their Figure 11): although the MDs of TDW and TDE show a similar shape to the MDs of the thin disk, the former are systematically more metal-poor than the latter, even taking into account the likely effect of adopting the different theoret-

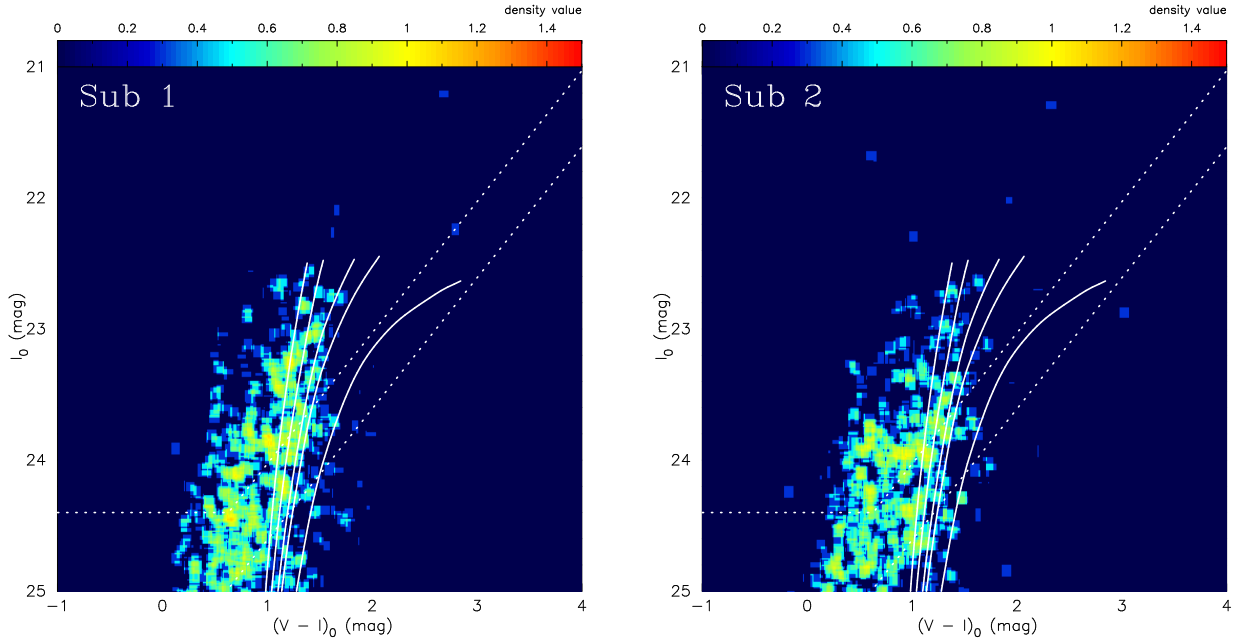


FIG. 8.— $[(V - I)_0, I_0]$ CMDs for stellar-like sources in the two substructure regions, Sub 1 (left) and Sub 2 (right), of NGC 55’s halo. The solid lines are theoretical isochrones (VandenBerg et al. 2006) of age 12 Gyr and $[\alpha/\text{Fe}] = +0.3$ spanning the metallicity range $[\text{Fe}/\text{H}] = -2.31, -1.71, -1.31, -1.14$ and -0.71 . The dotted lines denote the full ranges of the 50% and 80% completeness levels.

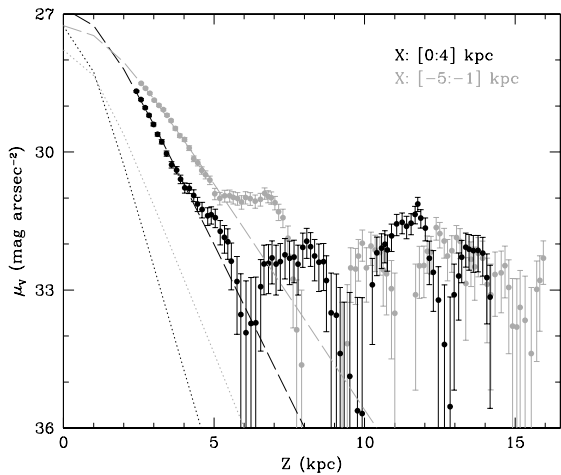


FIG. 9.— The surface brightness profile in the perpendicular direction to the galactic plane at a restricted x range, for the north-western (black) and north-eastern (gray) region of NGC 55. The long-dashed lines denote the model distributions of old RGB stars in the form of a locally isothermal disk model with a scale height of $z_{0,\text{RGB}}^{\text{W}} = 1635 \pm 30$ pc (black) and $z_{0,\text{RGB}}^{\text{E}} = 2203 \pm 25$ pc (gray), respectively. The dotted lines denote those of AGB stars with a scale height of $z_{0,\text{AGB}}^{\text{W}} = 969 \pm 62$ pc (black) and $z_{0,\text{AGB}}^{\text{E}} = 1341 \pm 60$ pc (gray), respectively. The background levels for RGB and AGB stars are $\mu_{V,\text{back}}^{\text{RGB}} \sim 30.8 \pm 0.1$ mag arcsec $^{-2}$ and $\mu_{V,\text{back}}^{\text{AGB}} \sim 33.6 \pm 0.1$ mag arcsec $^{-2}$, respectively.

ical model of stellar evolution and somewhat large photometric errors in Seth et al. (2005b). This may suggest some population difference between our detected thick disk and the inner thin disk in NGC 55.

We also note that the MD in the individual region of NGC 55 shows a slightly different profile from each

other: the MD of Sub 1 seems to show a higher fraction of metal-poor stars than that of Sub 2 and the MD of TDE has slightly a smaller fraction of metal-poor stars with $[\text{Fe}/\text{H}] \lesssim -2$ than that of TDW. These differences in MDs may reflect different stellar population in each substructure. To quantify the difference in these MDs, we employ a two-sided Kolmogorov-Smirnov (KS) test for the cumulative form of MDs. The calculated KS probability for the null hypothesis that all of the four populations originate from the same stellar population is only less than 1%: this is a maximum probability for all of the KS tests. Thus, these MDs are statistically different, thereby implying that stellar population in each substructure is different. However, we note that we cannot get rid of the degeneracies between metallicity and age when using isochrones to infer metallicity.

6. DISCUSSION AND CONCLUDING REMARKS

Our Suprime-Cam observation of NGC 55 has revealed that this late-type galaxy holds extended galactic structures well beyond its bright disk component, namely TDE, TDW, Sub 1, Sub 2, and a diffuse halo. We discuss here the possible origin of these extended components in NGC 55.

As already shown in Section 5, the stellar population in each of these structures seems to be statistically different from each other, as deduced from the analysis of these MDs. However, taking into account the spatial distribution of Sub 1 and Sub 2 as well as the difference of stellar populations between TDE and TDW, there is a possibility that both Sub 1 and Sub 2 may be associated with some merging event which also gives rise to disk thickening in its east part. If this conjecture is the case, then the MD of TDE should be a combination of the MD of TDW and that of either Sub 1 or Sub 2, which is however unlikely as it follows from Figure 10. Thus, the

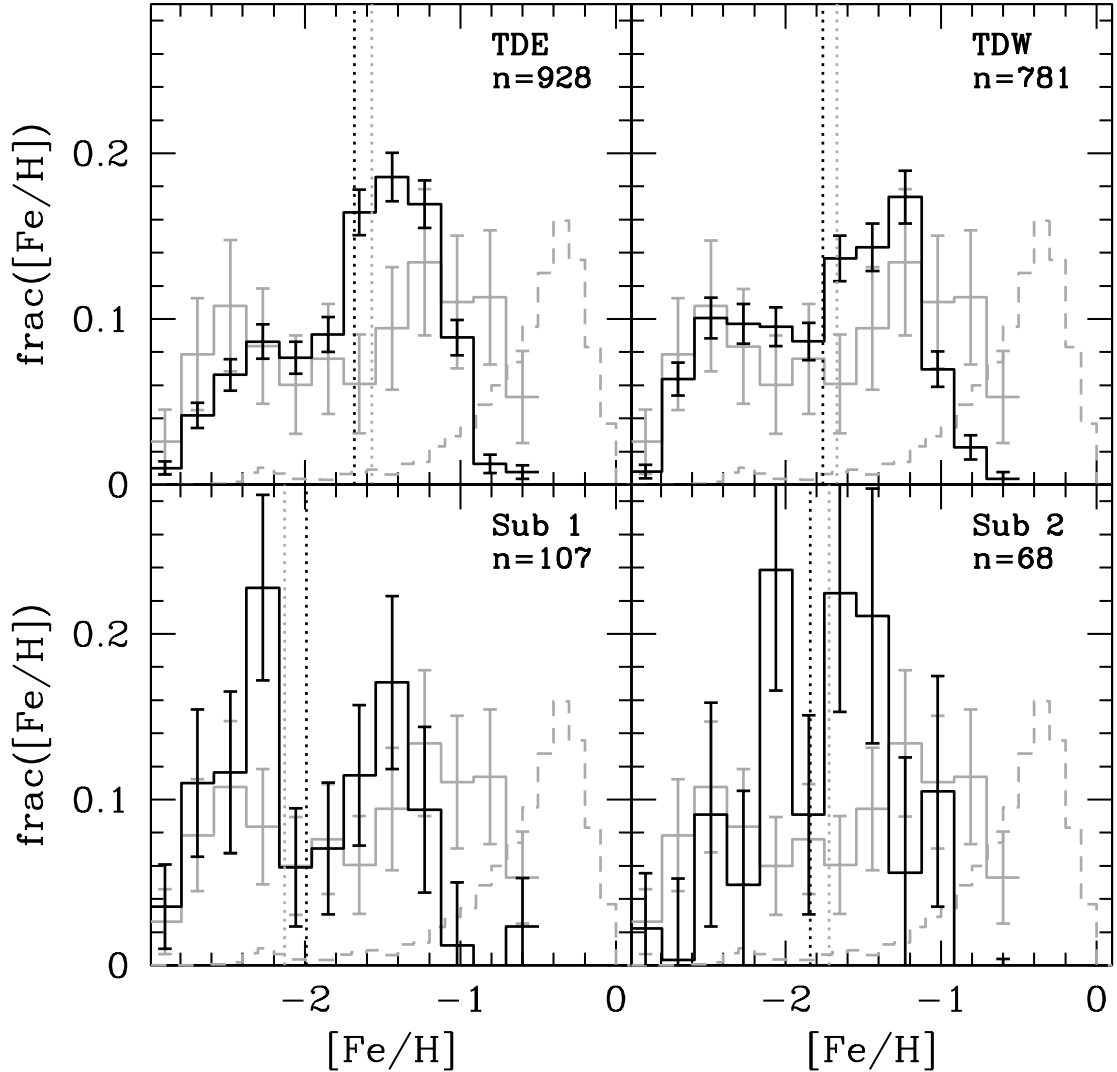


FIG. 10.— Metallicity distributions for the thick disk (upper panels) and substructures (lower panels). The number of stars used to derive these are shown in the upper right corner of each panel. Gray histograms correspond to the MD of the control field consisting of 69 objects and gray dashed histograms correspond to the MD of M31’s Giant Southern Stream obtained by Tanaka et al. (2010), which is not sensitive to the $[\text{Fe}/\text{H}] > -0.7$ metallicities. The vertical dotted lines show the mean metallicity (black) and median metallicity (gray) of each field.

TABLE 2
FUNDAMENTAL PROPERTIES OF THE SUBSTRUCTURES

Name	μ_V (mag arcsec $^{-2}$)	$[\text{Fe}/\text{H}]_{\text{mean}}$ (dex)	Standard Div. (dex)	$[\text{Fe}/\text{H}]_{\text{med}}$ (dex)	Quartile Div. (dex)	Error (dex)
Thick Disk East	29.0 ± 0.03	-1.68	0.54	-1.57	0.37	0.14
Thick Disk West	28.7 ± 0.02	-1.76	0.58	-1.67	0.46	0.14
Substructure 1	30.8 ± 0.11	-1.99	0.59	-2.13	0.43	0.13
Substructure 2	31.2 ± 0.17	-1.84	0.42	-1.72	0.30	0.13

difference in stellar populations between TDE and TDW may be attributed to another merging event, which is not related to the origin of Sub 1 and Sub 2.

Next, we compare the stellar populations of NGC 55’s substructures with those of M31’s halo. The MDs of

NGC 55’s substructures show a very different shape from those of M31’s Giant Southern Stream, thereby suggesting that stellar population is quite different between NGC 55 and M31. Furthermore, the MDs of other substructures in M31 such as Stream C and D with low stel-

lar density (Tanaka et al. 2010) are also different from those of NGC 55. These results may suggest the difference in the formation processes of stellar halos among different Hubble types of galaxies.

Previous studies of M31’s stellar halo show a positive correlation between metal abundance and surface brightness for substructures observed in M31’s halo (Gilbert et al. 2009; Tanaka et al. 2010), i.e., tidal debris with higher surface brightness tend to be more metal-rich. This correlation implies that tidal debris with higher surface brightness may originate from more luminous and thus metal-rich dwarf satellites, and/or more recent encounters. For NGC 55’s substructures, a similar correlation can be seen as shown in Figure 11, although the trend is systematically shifted toward a more metal-poor end than that for M31’s halo. Thus, NGC 55’s stellar halo may have formed through merging of relatively metal-poor dwarf galaxies compared to M31’s stellar halo. Provided that the mass-metallicity relation of dwarf galaxies in the Sculptor Group is the same as that observed in the Local Group Côté et al. (2000), NGC 55’s halo may have originated from less massive dwarf galaxies than those for the formation of M31’s halo, thereby implying that NGC 55 itself is less massive than M31 at the current epoch. This seems to be in agreement with the properties of M33 as well: this late-type galaxy has a less massive halo than M31 and has some faint substructures with metal-poor and low surface brightness in its halo (McConnachie et al. 2010).

The current study thus suggests that galaxies with different Hubble types have different properties of stellar halos as characterized by different metallicity and surface brightness in their substructures. However stellar halos in earlier Hubble types have yet been unidentified, simply because there are only few such early-type galaxies in the local volume so that current telescopes are able to resolve stars. On the other hand, a variety of substructures in the form of tidal streams have been found around more distant galaxies, where it is noteworthy that morphologies of tidal streams between early and late type galaxies are quite different (e.g., Peng et al. 2002; Martínez-Delgado et al. 2010). Resolving these substructures into individual stars by, e.g., Thirty Meter Telescope and/or Extremely Large Telescope, would provide further insights into the formation and evolution of stellar halos as a function of the Hubble sequence.

As part of our survey of stellar halos in external galaxies, we have observed the north part of the stellar halo in NGC 55, using deep and wide-field *V*- and *I*-band images taken with Subaru/Suprime-Cam. On the basis of the analysis of the CMDs compared with theoretical isochrones, we have obtained the following major results:

1. We have found that the stellar populations at $z \gtrsim 5$ kpc above the disk plane are dominated by old RGB stars with lower metallicity than M31 and the Milky Way. We derive a TRGB-based distance modulus to the galaxy of $(m - M)_0 = 26.58 \pm 0.11$ ($d = 2.1 \pm 0.1$ Mpc).
2. Based on the density map of NGC 55’s stellar populations, we have found asymmetric thick disk features in the north region of NGC 55, which we refer to as TDE for a disturbed thick disk in the

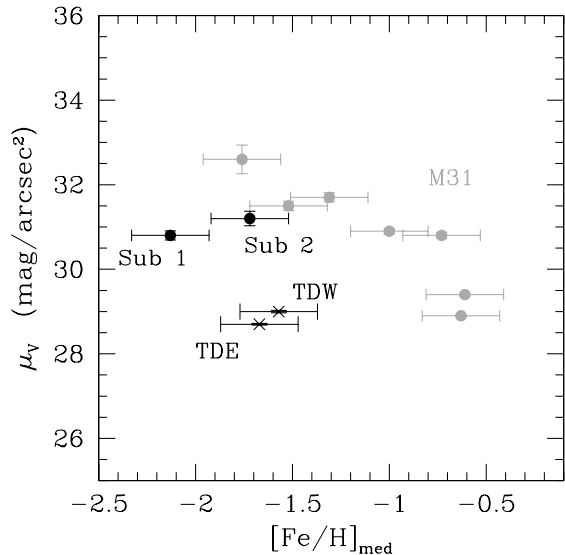


FIG. 11.— The median metallicity against surface brightness for the substructures of NGC 55 (filled black circles) and M31 (filled gray circles). Black crosses denote the disturbed and undisturbed thick disk structures of NGC 55. Metallicity uncertainties (± 0.2 dex) are derived from the error analysis given in Tanaka et al. (2010). It follows that tidal debris with higher surface brightness tend to be more metal-rich in both galaxies and that NGC 55’s trend is systematically shifted towards a more metal-poor end than that for M31’s halo.

east and TDW for an undisturbed thick disk in the west. We have also identified two overdense substructures at $z \sim 6.5$ kpc, which we refer to as Substructure 1 and 2 in this work. These substructures may correspond to remnants of merging events of small galaxies associated with the formation of NGC 55’s halo.

3. Detailed comparisons between the photometric data for halo regions of NGC 55 and that of the control field suggest the presence of a diffuse metal-poor halo extended out to at least $z \sim 16$ kpc. However, it is yet unclear to what extent this faint component is actually distributed.
4. The stellar density distribution perpendicular to the galactic plane of NGC 55 is described by a locally isothermal disk at $z \lesssim 6$ kpc and a diffuse metal-poor halo with $\mu_V \gtrsim 32$ mag arcsec⁻² at higher z , where old RGB stars dominate.
5. From the photometric comparison of RGB stars with the theoretical stellar evolutionary model, we have obtained the MDs in the extraplanar regions. Both TDE and TDW show the peak, average and median metallicity of $[\text{Fe}/\text{H}]_{\text{peak}} \sim -1.4$, $[\text{Fe}/\text{H}]_{\text{mean}} \sim -1.7$ and $[\text{Fe}/\text{H}]_{\text{med}} \sim -1.6$, respectively. In contrast, Substructure 1 and 2 show more metal-poor features than the thick disk structures. Furthermore, the low KS probabilities indicate that all the MDs are statistically different, suggesting that the stellar population in each substructure may have a different origin.

Data reduction and analysis were carried out on general common use computer system at ADAC (Astronomical Data Analysis Center) of the National Astronomical Observatory of Japan. This work has been supported in

part by a Grant-in-Aid for Scientific Research (20340039) of the Ministry of Education, Culture, Sports, Science and Technology in Japan.

REFERENCES

- Abadi, M. G., et al. 2003, *ApJ*, 597, 21
Bullock, J. S., & Johnston, K. V. 2005, *ApJ*, 635, 931
Carollo, D., et al. 2007, *Nature*, 450, 1020
Côté, S., et al. 1997, *AJ*, 114, 1313
Côté, P., et al. 2000, *ApJ*, 533, 869
Davidge, T. J. 2005, *ApJ*, 622, 279
Dean, J. F., Warren, P. R., & Cousins, A. W. J. 1978, *MNRAS*, 183, 569
Engelbracht, C. W., et al. 2004, *ApJS*, 154, 248
Ferguson, A. M. N., et al. 1996, *AJ*, 112, 2567
Gilbert, K. M., et al. 2009, *ApJ*, 701, 776
Guhathakurta, P., et al. 2005, *astro-ph/0502366*
Hummel, E., Dettmar, R. J., & Wielebinski, R. 1986, *A&A*, 166, 97
Ibata, R., et al. 2007, *ApJ*, 671, 1591
Jerjen, H., Binggeli, B., & Freeman, K. C. 2000, *AJ*, 119, 593
Kalirai, J. S., et al. 2006, *ApJ*, 648, 389
Kauffmann, G. 1996, *MNRAS*, 283, 117
Martínez-Delgado, D., et al. 2010, *AJ*, 140, 962
McConnachie, A. W., et al. 2010, *astro-ph/1009.2804*
Miyazaki, S., et al. 2002, *PASJ*, 54, 833
Ouchi, M., et al. 2004, *ApJ*, 611, 660
Peng, E. W., et al. 2002, *AJ*, 124, 3144
Puche, D., Carignan, C., & Wainscoat, R. J. 1991, *AJ*, 101, 447
Salaris, M., & Cassisi, S. 2005, *Evolution of Stars and Stellar Populations* (New York: Wiley)
Schlegel, D. J., Finkbeiner, D. P., & Davis, M. 1998, *ApJ*, 500, 525
Seth, A. C., Dalcanton, J. J., & de Jong, R. S. 2005a, *AJ*, 129, 1331
Seth, A. C., Dalcanton, J. J., & de Jong, R. S. 2005b, *AJ*, 130, 1574
Stetson, P. 1987, *PASP*, 99, 191
Tanaka, M., et al. 2010, *ApJ*, 708, 1168
Tikhonov, N. A., Galazutdinova, O. A., Drozdovsky, I. O. 2005, *A&A*431, 12
VandenBerg, D. A., Bergbusch, P. A., & Dowler, P. D. 2006, *ApJS*, 162, 375
van der Kruit, P. C., & Searle, L. 1981, *A&A*, 95, 105
Yagi, M., et al. 2002, *AJ*, 123, 66
Yanny, B., et al. 2000, *AJ*, 540, 825
Yoachim, P., & Dalcanton, J. J. 2006, *AJ*, 131, 226